Applied Surface Science 320 (2014) 718–724

Contents lists available at ScienceDirect

Applied Surface Science

journal homepage: www.elsevier.com/locate/apsusc

Electrochemical behavior and biological response of Mesenchymal Stem Cells on cp-Ti after N-ions implantation

M. Rizwan[a], A. Ahmad[a], K. M. Deen[b], W. Haider[c,*]

[a] Department of Metallurgical & Materials Engineering, University of Engineering & Technology, 54890 Lahore, Pakistan
[b] Corrosion Control Research Cell, Department of Metallurgy & Materials Engineering, CEET, University of the Punjab, 54590 Lahore, Pakistan
[c] Mechanical Engineering Department, University of Texas Pan American, Edinburg, TX 78539 USA

ARTICLE INFO

Article history:
Received 21 July 2014
Received in revised form
25 September 2014
Accepted 26 September 2014
Available online 6 October 2014

Keywords:
Corrosion
Ions implantation
Electrochemical
STEM cells

ABSTRACT

Titanium and its alloys are most widely used as implant materials due to their excellent biocompatibility, mechanical properties and chemical stability. In this study Nitrogen ions of known dosage were implanted over cp-Ti by Pelletron accelerator with beam energy of 0.25 MeV.The atomic force microscopy of bare and nitrogen implanted specimens confirmed increase in surface roughness with increase in nitrogen ions concentration. X-ray diffraction patterns of ions implanted surfaces validated the formation of $TiN_{0.3}$ and Ti_3N_{2-x} nitride phases. The tendency to form passive film and electrochemical behavior of these surfaces in ringer lactate (RL) solution was evaluated by Potentiodynamic polarization and electrochemical impedance spectroscopy respectively. It is proved that nitrogen ions implantation was beneficial to reduce corrosion rate and stabilizing passive film by increasing charge transfer resistance in RL. It was concluded that morphology and proliferation of Mesenchymal Stem Cells on nitrogen ions implanted surfaces strongly depends on surface roughness and nitride phases.

1. Introduction

Titanium and its alloys are commonly used for biomedical applications. These materials have remarkable characteristics of high strength to weight ratio and good performance in biological environment. Titanium has inherent tendency to form passive film at the surface which prevent direct contact with biological environment [1]. For orthopedics bone reconstruction in the presence of TiO_2 oxide film has great importance for efficient osteo-integration. The chemical interaction of amino acids and inorganic species within body fluids with TiO_2 passive film may enhance dissolution of metal ions from the surface thus reducing bio-integration of titanium implant [2–4]. The metal ions presence at the vicinity of implant may initiate local inflammatory reactions within surrounding tissues. The inflammation and irritation effects may appear due to surface topography, tri-biological behavior and surface chemistry of implant. These side effects may be overcome by surface modifications with ion beam implantation in order to improve biocompatibility [5]. Many efforts have been made in the past to modify surfaces by anodic oxidation [6], sol-gel method [7,8], physical vapor deposition [9,10], chemical vapor deposition [11] and thermal oxidation [12].By using these techniques the surface modification of implants has limited the dissolution of metal ions into the surrounding tissues and to enhance bone/metal integration. Surface modification by implanting ions on the surface of titanium alloys may have great influence on passive film structure and its self-healing properties [13]. Schultze et al. [14] described the implantation of Palladium, Iron and Xenon to modify the oxide films of Hafnium and Titanium. Ions implantation could also improve the overall stability, corrosion resistance; wear resistance which could enhance implant–tissue interactions. It is reported that implantation of 'Mg' ions on titanium surface could enhance the proliferation and adhesion capacity of human Mesenchymal Stem Cells [15,16]. To achieve better osteo-integration and tendency of bone cells to attach at the surface of titanium after 'Kr', 'Ar', 'Ne' and 'Xe' ions implantation was also assessed by Braceras et al. [17]. The high bioactivity and better electrochemical response of titanium surface was achieved by 'Ca' ions implantation. The formation of apatite was evident on cp-Ti after calcium ions implantation which could be beneficial for better osteo-integration and cell proliferation [18]. In support to this study it has been found that the diffusion of nitrogen by microwave assisted chemical deposition process could be beneficial for better biological response of titanium alloy surfaces [19]. The nitrogen ions implantation on titanium surface produced titanium nitride phases, which could provide excellent superficial mechanical strength, higher corrosion resistance and lower

* Corresponding author. Tel.: +1 9566653691.
E-mail address: haiderw@utpa.edu (W. Haider).

http://dx.doi.org/10.1016/j.apsusc.2014.09.169
0169-4332/

cytotoxicity when come in interaction with human pre-osteoblast cells [20].

Previous studies also showed that morphology of MSCs, osteoblast and fibroblast cells on implant surface always depend on the physical and chemical properties of the surface. The differentiation and proliferation of MSCs as a function of surface morphology and chemistry has been explored and evaluated on TiO_2 nanotubular structure. The conversion of MSCs into osteoblast cells was more effective on smaller size TiO_2 nanotubular structure [21–24].

The present research work is mainly focused to enhance corrosion resistance of commercially pure titanium in simulated body fluid by nitrogen ions implantation. The morphology and proliferation of Mesenchymal Stem Cells (MSCs) was evaluated to investigate the biological response of nitrogen implanted surfaces. The effect of nitrogen ions dosage and surface roughness on morphology and proliferation of MSCs was determined for their compatibility and integration for orthopedic applications.

2. Experimental

In this study the commercially pure Titanium grade 2 (cpTi-2) metal having chemical composition 0.49 wt.% Fe, 0.01 wt.% Ni and balance Ti was used as substrate. The specimens (5 mm × 5 mm × 10 mm) were wire cut form a plate. Top surface of these specimens was ground by silicon carbide paper successively from 120 to 1000 grit size followed by polishing with diamond paste of different grade down to 1 μm particle size. These specimens were exposed to Nitrogen ions beam (0.25 MeV) at room temperature in a Pelletron Accelerator. The polished cpTi-2 specimens were targeted by nitrogen ion beam at 75 nA/cm^2 and 130 nA/cm^2 for 3 and 10 min, respectively. The dose of nitrogen ions per unit area was determined by using equation (1) as follows:

$$\frac{\text{Ions}}{\text{Area}} = \frac{iXT}{q} \quad (1)$$

where '*i*' is the beam current density (A/cm^2), '*T*' is the exposure (seconds) and '*q*' is the charge on an ion (1.6×10^{-19} C/ion). The corresponding nitrogen ions (N^{2+}) dosage per unit area at each current density was calculated as 8.437×10^{13} ions/cm^2 and 4.875×10^{14} ions/cm^2 .Three specimens at each dose were prepared and designated as B-13 and B-14, respectively.

The surface features of bare (B-01), B-13 and B-14 were revealed by atomic force microscope (Veeco CP-II). The morphology and surface roughness was determined to correlate with electrochemical surface reactions and *in vitro* cell proliferation.

The XRD patterns were obtained by using X Pert PRO MPD θ–2θ diffractometer. The X-ray generator was operated at 40 kV and tube current was fixed at 40 mA by using Cu K_α (1.540598 Å) radiation source. The surface morphology of B-01, B-13 and B-14 was determined by atomic force microscopy (AFM). The effects of ions bombardment on cpTi-2, the surface profile was measured quantitatively by AFM which was operated in a contact tip mode.

The corrosion potential measurement, potentiodynamic polarization and electrochemical impedance spectroscopy (EIS) were carried out in a three electrode cell system connected to Gamry Potentiostat PC-14/750. Ion implanted specimens (B-13 and B-14) (1.5 cm^2) were immersed in ringer lactate (RL) solution (Na^+: 130 M, K^+: 0.0054 M, Ca^+: 0.00184 M, Cl^-: 0.1118 M, HCO_3^-:0.0272) as working electrode, graphite rod was used as counter and saturated calomel electrode (SCE) acted as reference electrode. For potentiodynamic polarization scan the specimens were polarized from −0.5 V to +2.0 V with respect to open circuit potential (OCP) with a scan rate of 5 mV/sec. The EIS spectra were obtained in the same electrolyte by perturbing ac potential of 10 mV within a frequency range of 0.01 Hz–100 kHz.

The Mesenchymal Stem Cells (MSCs) also known as osteo-Progenitor Cells were isolated from the femur of 8 week old female Wistar rat. The femur was surgically removed and adhering soft tissues were cleaned, bone was cut aseptically from the edges and bone marrow was flushed out with the help of syringe containing 10 ml Dulbecco's Modified Eagle Medium (DMEM). The bone marrow cells were disrupted by passing it several times through 16 gauge needle. 1 ml of Fetal Bovine Serum (FBS) was added to 10 ml bone marrow which was flushed and spun at 450 Hz for 5 minutes at room temperature. Supernatant was removed and cells were re-suspended in complete medium (DMEM containing Glutamine, 10% FBS, 100 U/ml penicillin, and 100 μg/ml streptomycin). 5×10^5 cells were added in 25 cm^2 cell culture flask. The cells were incubated under standard culture conditions for 24 h, washed with Physiological Body Solution (PBS) to remove non adherent cells followed by addition of complete medium. The cells at second passage were used for further experimentation.

Initially 1×10^4 MSCs were added in 6-well cell culture plate containing 3 ml medium (DMEM containing glutamine, 10% FBS, 100 U/ml penicillin, and 100 μg/ml streptomycin). Sterilized metal specimens (heated at 180 °C for 30 min) were seeded into the well immediately and labeled accordingly. These systems were incubated at 37 °C with 5% CO_2 in humidified environment for 24 and 48 h, respectively. The cells morphologyon bare and nitrogen ions implanted titanium surface was examined by bright field microscopy.

3. Results and discussion

3.1. Surface morphology

The surface topography of bare (B-01) and nitrogen ion implanted surfaces (B-13, B-14) was revealed by Atomic Force Microscope as shown in Fig. 1a–c, respectively. The roughness of bare; B-01, B-13 and B-14 was determined from average values of parameters i.e. average roughness (R_a), maximum height of the profile (R_y), ten point height of irregularities (R_z) and mean width of the profile elements (R_{sm}) as exhibited in Table 1. It was validated by the average roughness (R_a) of B-01, B-13 and B-14 specimens was 8.79 nm, 81.32 nm and 84.86 nm, respectively.

Bombardment of 0.25 MeV nitrogen ion beam deteriorated the surface finish by producing nonhomogeneous asperity structure. The increase in beam current density and exposure time also promoted erosion of the surface. The development of this profile was attributed to the elastic and inelastic collisions of nitrogen ions with the surface atoms. At low dose (B-13) formation of conical structure was sharp due to sputtering of ions and erosion process. At higher ions dosage, the relatively higher current ions beam further damaged the surface by deforming asperities. The surface structure disorderness was more pronounced in B-14 than B-13 and B-01 specimen. However the difference of average roughness (R_a) was low between B-13 and B-14 due to the deformation of random rough surface morphology by the incident energetic nitrogen ions at high current. The higher mean width of the profile elements (peaks and valley) (R_{sm}) of B-14 also validated the maximum damage at the surface with increase in ions dose. The high kinetic energy and small atomic radii of nitrogen ions than Ti atoms could also induce structural distortions within the crystal

Table 1
Surface profile parameters of bare and ions implanted cpTi-2.

Specimens	R_a (nm)	R_y (nm)	R_z (nm)	R_{sm} (nm)
B-01	8.79	105.73	46.13	177.45
B-13	84.91	430.18	219.30	916.23
B-14	90.95	484.20	315.33	997.62

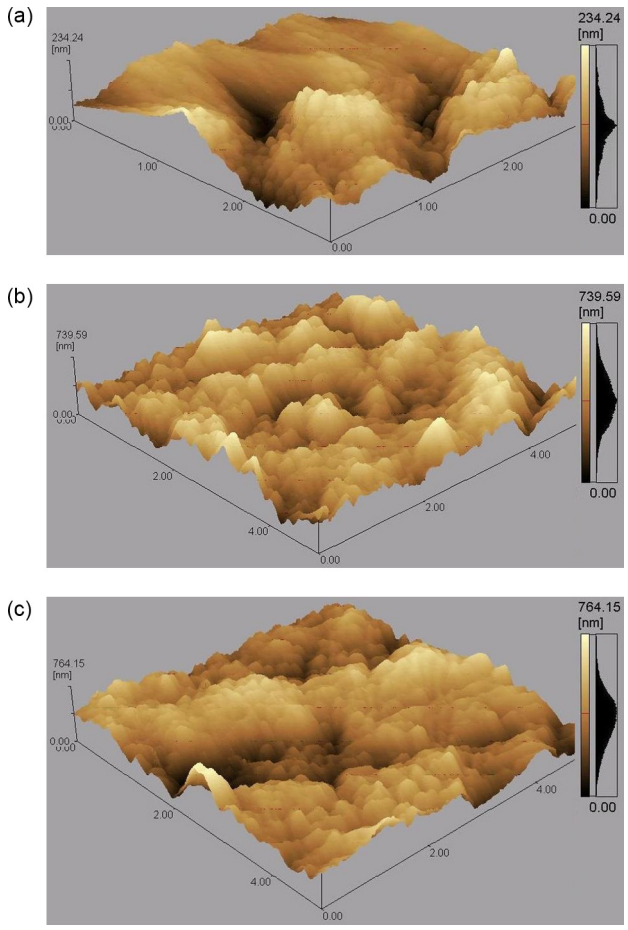

Fig. 1. Atomic force microscope images depicting surface morphology of bare (a) B-01 and nitrogen ions implanted specimens (b) B-13, (c) B-14.

lattice at or near the surface regions. The diffusion of nitrogen ions could also promote the formation of nonmetallic phases within the surface.

3.2. X-ray diffraction

The x-rays were produced from kα-Cu anode and specimens were scanned from angle (2θ) 20° to 70° with a step size of 0.05°/sec. The XRD pattern of B-13 and B-14 confirmed the presence of coherent hexagonal titanium nitride ($TiN_{0.3}$) phase which was observed at $2\theta = 39.875°$, 52.625° and 62.675° (with slight shift in diffraction peaks from reference JCPDS code 00-041-1352) in α-Ti matrix as shown in Fig. 2. The crystal lattice parameters of $TiN_{0.3}$ phase ($a = b = 2.9737$ Å, $c = 4.7917$ Å) were nearly similar to the α-Ti lattice parameters. The distortion in crystal lattice was evident by the slight shift in XRD peaks due to the formation of non-coherent rhombohedral Ti_3N_{2-x} phase within alpha titanium (as per JCPDS 00-040-0958). This additional phase may produce significantly large distortion in the crystal lattice because the ratio of long to short edge of unit cell 'c/a' approached to 7.285 without any marked variation in 'a' and 'b' which could induce compressive stresses in the surrounding lattice structure and may disrupt the uniformity of alpha phase compared to $TiN_{0.3}$ phase having 'c/a' ratio 1.611. The depression in peak at 39.875° and sharp diffraction at 62.675° shown by B-14 was in confirmation of pronounced distortion in crystal lattice due to formation of non-coherent lattice phase.

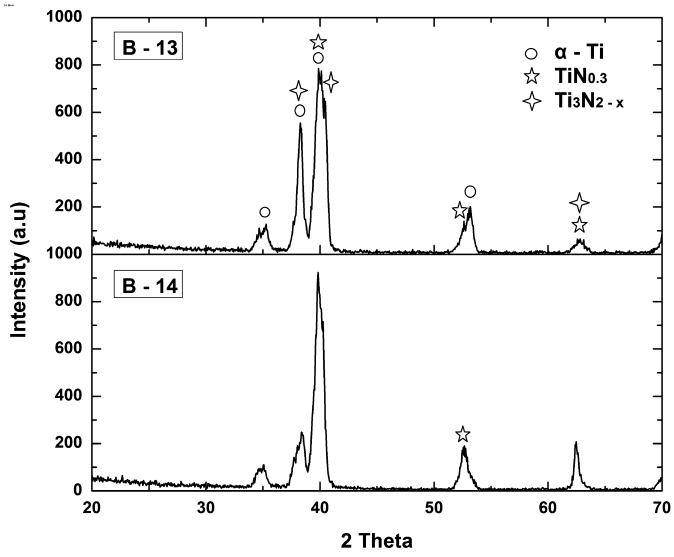

Fig. 2. XRD pattern of nitrogen ion implanted specimens.

3.3. Electrochemical characterization

3.3.1. Open circuit potential

The Open Circuit Potential $(OCP)_{SCE}$ of B-01 when exposed to ringer lactate solution (RL) was more active (negative) than B-13 and B-14. Initially OCP of B-01 was −493.79 mV which shifted to more negative potential (−523.01 mV) after 300 min during immersion in RL solution. The OCP of B-13 specimen was relatively less electronegative (−257.57 mV) initially upon immersion into RL solution then it shifted to electronegative potential (−401.10 ± 0.05 mV) after 200 min and remained constant till 300 min. In contrast to B-01 and B-13, B-14 depicted positive potential (noble behavior) and rapidly moved to active side after about 40 min as shown in Fig. 3. The shift of potential in negative direction continued till 180 min followed by gradual achievement of constant potential (−319.16 ± 0.10 mV). Compared to B-13 the potential of B-14 specimens represented relatively less negative potential (more noble behavior) which is considered due to the formation of titanium nitride phases at the surface. The variation in potential

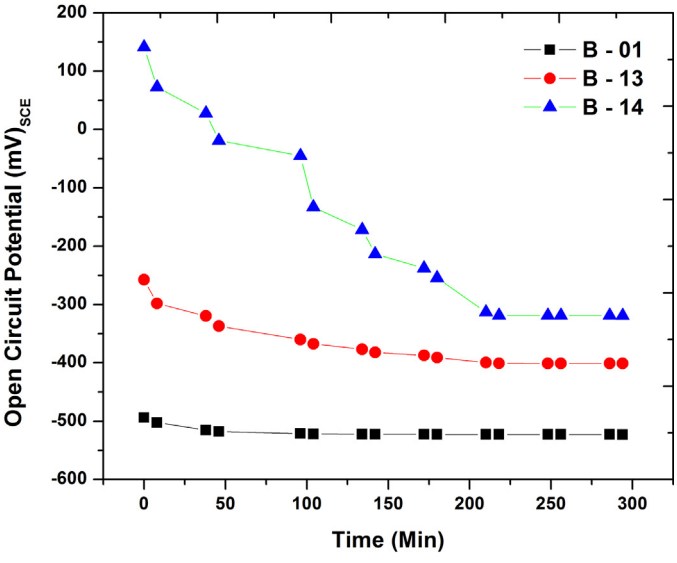

Fig. 3. Variation of open circuit potential (OCP) vs. time.

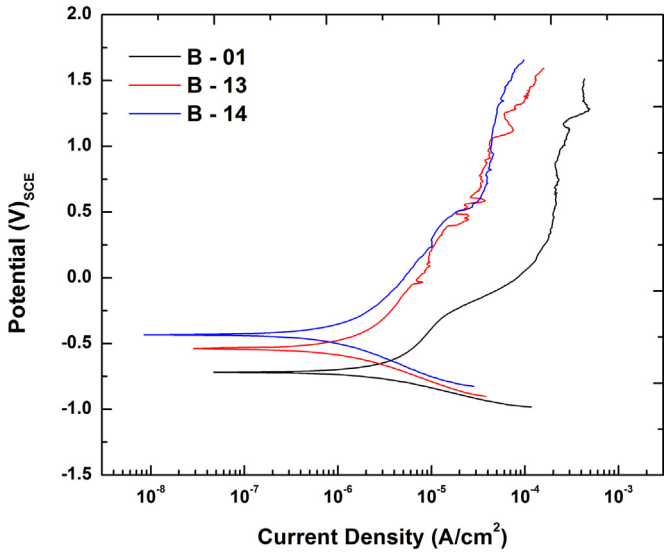

Fig. 4. Potentiodynamic polarization behavior of bare and ions implanted titanium substrates.

and shift towards active direction corresponded to inhomogeneity in the microstructure of the surface and roughness at nano scale, respectively. The bare specimen (B-01) showed greater tendency to dissolute in RL solution than nitrogen ions implanted specimens. It was also evident that corrosion tendency was reduced with increase in nitrogen ions dose on titanium surface.

3.3.2. Potentiodynamic polarization trends

The potentiodynamic scans of bare and ion implanted specimens were obtained in RL solution as shown in Fig. 4. It was observed that all specimens showed passive behavior in RL solution. The anodic current density of bare titanium specimen was relatively higher than N-implanted specimens. The kinetic parameters for the determination of dissolution tendency of these specimens were calculated by fitting the polarization curves in linear Tafel region and results are displayed in Table 2. It was found that corrosion potential (E_{corr}) shifted towards more negative direction than initially stabilized OCP. This represents the charge relaxation within the surface and ingress of cationic species in the electrolyte toward the surface during cathodic polarization.

The lower β_c value was in support to increase tendency of reduction reactions at the surface or dissolution of passive film. The decrease in anodic and cathodic Tafel slopes (β_a and β_c) show higher corrosion current density. The bare specimen was least corrosion resistant than nitrogen ions implanted specimens as depicted by higher corrosion current density and more active corrosion potential. The corrosion rate of nitrogen ions implanted specimens was approximately one half of the bare specimen. The formation of titanium nitride ($TiN_{0.3}$), and Ti_3N_{2-x} phases at the surface restricted electrochemical attack of simulated body fluid hence limited the dissolution of metal ions. The higher value of anodic Tafel slope (β_a) by B-13 and B-14 specimens supported the formation of passive film which was relatively more stabilized than bare specimen. The B-01 specimen beyond

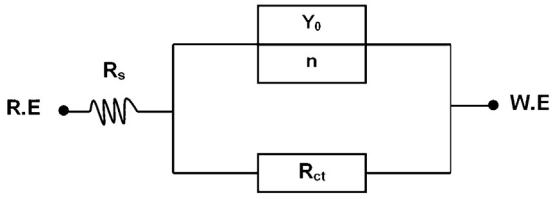

Fig. 5. The simulated equivalent electrical circuit model (EEC).

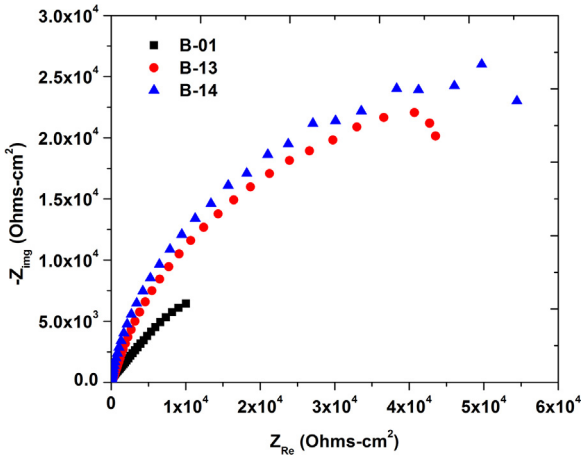

Fig. 6. Nyquist plots of bare and nitrogen ion implanted titanium specimens.

Tafel regime between potential −260.11 mV and +265.39 mV the current density increased from 1.61×10^{-5} to 1.75×10^{-4} A/cm^2, respectively. This behavior was followed by maintaining a constant (2.17×10^{-4} A/cm^2) current density attributed to formation of passive film. In case of B-13 beyond −68.04 mV, the small current excursions corresponded to localized reactions due to non-homogeneity and higher roughness of the surface after nitrogen ions bombardment. The B-14 specimen did not show these current excursions which depicted the formation of stable passive film. The shift of corrosion potential in less negative direction and anodic polarization trend toward lower current density after nitrogen ions implantation confirmed the least corrosion tendency by restricting dissolution of passive film. It was found that formation of nitride phases promoted corrosion resistance and reinforced the stability of formed passive films over titanium [20].

3.3.3. Electrochemical impedance spectroscopy

The Nyquist plots of bare and ion implanted surfaces were obtained by perturbing $(10\,mV)_{rms}$ potential at frequencies between 100 kHz - 10 mHz over surfaces in RL solution. The resultant single time constant loop spectrums were simulated to an equivalent electrical circuit model (EEC) as shown in Fig. 5.

The experimental values were fitted in EEC by EchemAnalyst software and obtained values are given in Table 3. The single time constant in Nyquist plots corresponded to charge transfer controlled electrochemical reactions at the surface by the ionic species of electrolyte as shown in Fig. 6. It was evaluated that charge transfer resistance 'R_{ct}' of B-01 (10.04 kΩ-cm^2) was low

Table 2
Potentiodynamic Tafel scans parameters for unexposed and nitrogen ions implanted specimens.

Specimen	Dose (ions/cm^2)	E_{corr} (mV)$_{SCE}$	β_a (V/decade)	β_c (V/decade)	I_{Corr} (μA/cm^2)	Corrosion rate (mpy)
B-01	Bare	−719	0.742	0.225	3.90	1.333
B-13	10^{13}	−537	0.806	0.330	1.78	0.608
B-14	10^{14}	−432	1.039	0.512	2.02	0.689

Table 3
Quantitative EIS modeling parameters obtained after fitting in equivalent electrical circuit.

Specimen	R_{ct} (kΩ-cm^2)	Y_o (S s^n)/cm^2	n
B-01	10.04	2.95×10^{-4}	0.95
B-13	43.54	2.80×10^{-6}	0.83
B-14	54.44	9.39×10^{-7}	0.65

compared to the resistance of B-13 and B-14. The 'R_{ct}' of B-13 was 43.54 kΩ-cm^2, which was about 4 times higher than the bare specimen. This increase in charge transfer resistance was due to the presence of nitride phases at the surface as confirmed by X-ray diffraction patterns. For specimen B-14, the 'R_{ct}' was further increased to 54.43 kΩ-cm^2 as given in Table 3. It was determined that by increasing the dose of nitrogen there was increase in charge transfer resistance which proved to be beneficial for enhancing

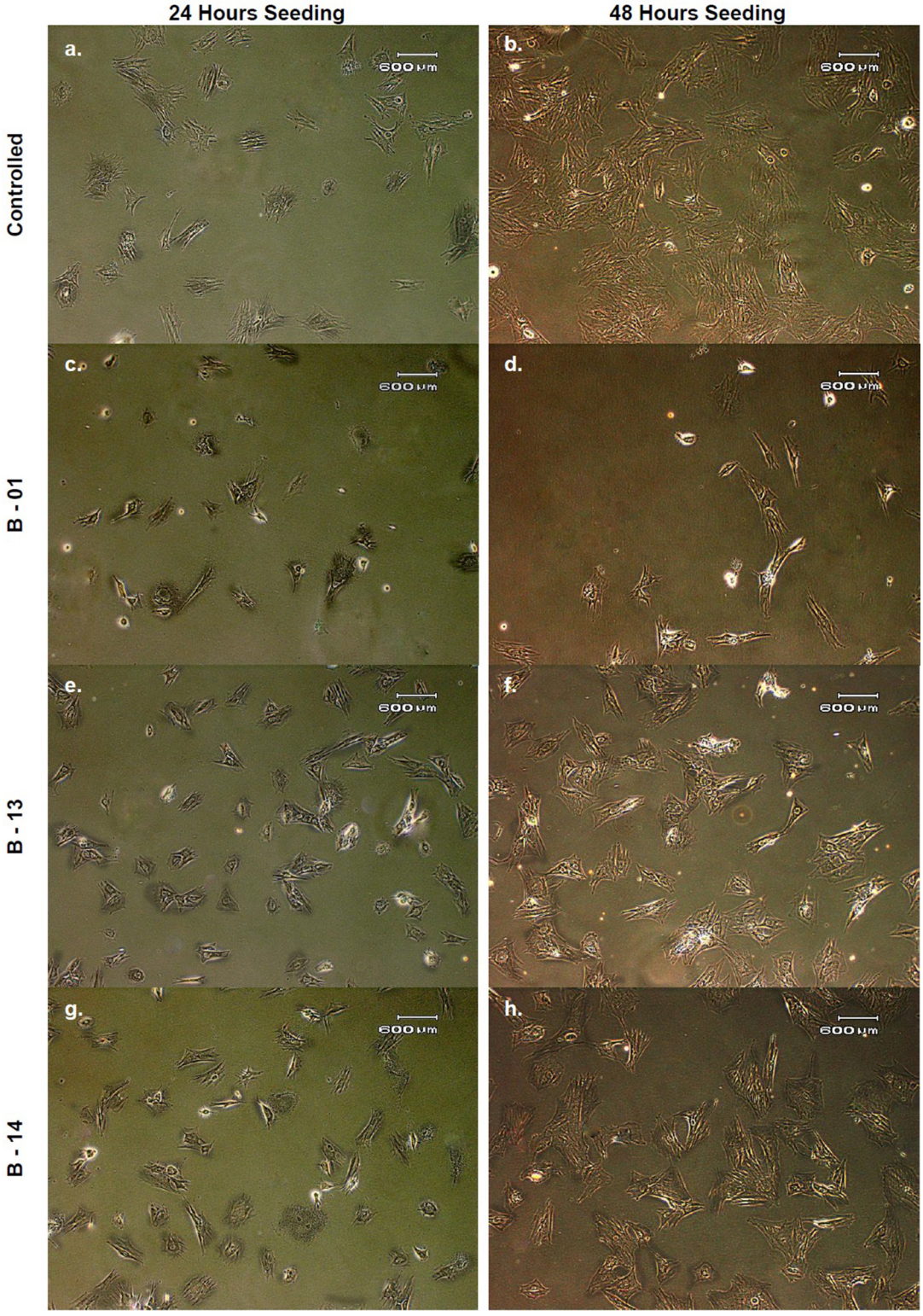

Fig. 7. The morphology of MSCs in fresh cell culture, control medium (a, b); on B-01 (c, d), B-13 (e, f) and B-14 (g, h) after 24 and 48 h.

corrosion resistance in RL solution. The higher dose of nitrogen ions also resulted in single time constant and increase in imaginary impedance component corresponded to lowering of constant phase element (CPE) which was directly related with the higher tendency of charge relaxation due to formation of barrier oxide film hence limited charge dissipation. The CPE was determined by using following equation

$$Y_{CPE} = \frac{1}{Z_{ing}(2\pi f)^n} \quad (2)$$

When relaxation coefficient 'n' is less than 1 it represents the non-ideal capacitive behavior and its value was inversely proportional to the nitrogen ion dose which morphologically disrupted the surface smoothness. The decrease in anodic current density and CPE shown by potentiodynamic curves and Impedance Spectra respectively were clear evidence of formation of stable passive film which restricted the approach of aggressive ions to the surface.

3.4. In-vitro response of Mesenchymal Stem Cells (MSCs)

Mesenchymal Stem Cells (MSCs) were cultured on bare and nitrogen ions implanted specimens of cp-Ti in order to investigate cells/metal interaction and proliferation after 24 and 48 h incubation periods. It was observed that there was little change in the morphology of cells on metal specimens implanted with nitrogen compared to controlled culture medium after 24 h exposure. However B-01 over which the cells become elongated and transformed into spindle shaped which depict the restricted growth and metabolic activity of MSCs.

On nitrogen ions implanted specimens the cells were proliferated over the surface and were comparable to control cells morphology whereas MSCs were shrunk on B-01. The least spreading tendency and round shape of MSCs confirmed the formation of cortical actin fibers at cells periphery [25]. After 48 h seeding of B-13 and B-14 specimens the MSCs were well spreaded over larger surface area and actin fibers appeared parallel to the long axis of cells similar to the morphology of cells in controlled medium as shown in Fig. 7. It is well known that spreading of cells correspond to organization and clustering of cytoskeleton and integrin receptors respectively which indicate higher stability of cells [26].

The total number of cells in controlled medium and metal specimen containing wells after 24 and 48 h incubation were counted by hemocytometer. It was determined that there was decrease in number of cells in metal containing wells after 24 h exposure compared to controlled medium. The proliferation of MSCs in B-01 specimen containing well was very poor and 47.2% cells were left in 24 h exposure followed by further decrease in concentration to 38.88% after 48 h. The growth of cells on B-13 was relatively better than over B-14 as shown in Fig. 8. There was also increase in number of MSCs after 48 h and approached to 83.33% compared to 75% cells viability during initial 24 h incubation on B-13. C.C. Chien et al. [27] also reported that cell proliferation over titanium was poor at surfaces with increased roughness. Cells adhesion and growth tendencies were in negative relation to the surface roughness parameters. Similarly in case of B-14 the increase in surface roughness due high dose of nitrogen ions restricted the growth of MSCs compared to B-13.

The formation of nitride phases at titanium surface facilitated the growth of MSCs in contrast B-01 but higher surface roughness adversely affected the cell proliferation in case of B-14 specimens.

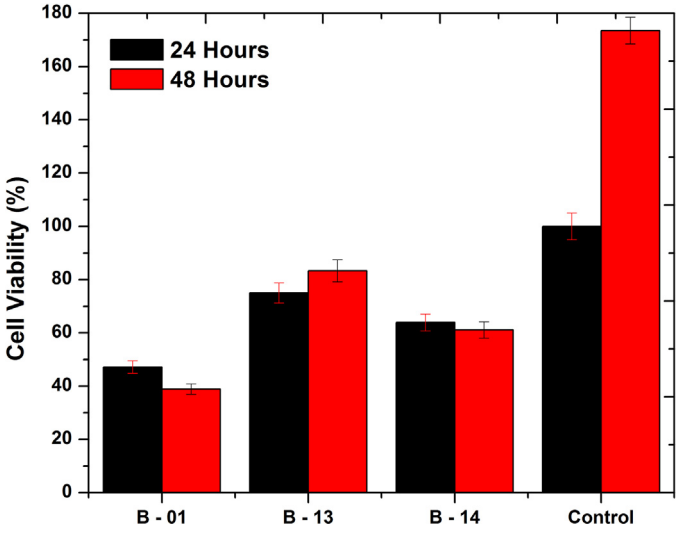

Fig. 8. Histogram showing the Cells proliferation over un-implanted and N-implanted specimens after 24 and 48 h.

4. Conclusions

It was concluded that increase in surface roughness was in direct relation with nitrogen ions dose. The XRD signatures confirmed the formation of coherent $TiN_{0.3}$ and rhombohedral Ti_3N_{2-x} phase in alpha titanium after nitrogen ions implantation. The shift of open circuit potential in noble direction and decrease in corrosion rate after N-ions dosage was in support to the results of impedance spectroscopy. The higher charge transfer resistance and decrease in constant phase element of B-14 specimen compared to B-13 related with the formation of nitride phases which limited the dissolution of titanium into the electrolyte. The degradation and restriction in the growth of Mesenchymal Stem Cells on B-01 and B-14 was considered as incompatibility of bare surface and higher surface roughness due to interaction of high dose ions beam with titanium, respectively.

References

[1] ToehSweeHin, Engineering Materials for Biomedical Applications, Vol. 1, World Scientific Publishing Co, 2004.
[2] S.M.A. Hosseini, M. Salari, M. Quanbari, Electrochemical behavior of Ti–alloy in the mixture of formic and phosphoric acid in the presence of organic compound, Int. J. Electrochem. Sci. 2 (2007) 935–946.
[3] Y. Mu, T. Kobayashi, M. Sumita, A. Yamamoto, T. Hanawa, Metal ion release from titanium with active oxygen species generated by rat macrophages in vitro, J. Biomed. Mater. Res. 49 (2000) 238–243.
[4] Shinji Takemoto, AkinoriTasaka, Masayuki Hattori, Kaoru Sakurai, O.D.A. Yutaka, Discoloration of Ti-20Cr alloy in oral environment and its surface characterization, Dental Mater. J. 31 (6) (2012) 1060–1067.
[5] T.R. Rautray, R. Narayanan, K.H. Kim, Ion implantation of titanium based biomaterials, Prog. Mater. Sci. 56 (2011) 1137–1177.
[6] J. Sun, Y. Han, K. Cui, Microstructure and apatite forming ability of the MAO-treated porous titanium, Surf. Coat. Technol. 202 (2008) 4248–4256.
[7] D.B. Haddow, S. Kothari, P.F. James, R.D. Short, P.V. Hatton, R.V. Noort, Synthetic implant surfaces 1. The formation and characterization of sol-gel titania films, Biomaterials 17 (1996) 501–507.
[8] L. Gan, J. Wang, R.M. Pilliar, Evaluating interface strength of calcium phosphate sol–gel-derived thin films to Ti6Al4V substrate, Biomaterials 26 (2005) 189–196.
[9] S.W.K. Kweh, K.A. Khor, P. Cheang, An in-vitro investigation of plasma sprayed hydroxyapatite (HA) coatings produces with flam spherodized feedstock, Biomaterials 23 (2002) 775–785.
[10] D. Krupa, J. Baszkiewicz, J. Zdunek, J. Smolik, Z.Z. Słomka, J.W. Sobczak, Characterization of the surface layers formed on titanium by plasma electrolytic oxidation, Surf. Coat. Technol. 205 (2010) 1743–1749.
[11] D.V. Shtansky, N.A. Gloushankova, I.A. Bashova, M.I. Petrzhik, A.N. Sheveiko, F.V.K. Kiryukhantsev, Multifunctional biocompatible nanostructured for load bearing implants, Surf. Coat. Technol. 201 (2006) 4111–4118.
[12] M.C. Garcia-Alonso, L. Saldan, G. Valles, J.L. Gonzalez-Carrasco, J. Gonzalez-Cabrero, M.E. Martinez, In-vitro corrosion behavior and osteoblast response of thermally oxidized Ti6Al4V alloy, Biomaterial 24 (2003) 19–26.
[13] P. Sioshansi, E.J. Tobin, Surface treatment of biomaterials by ion beam process, Surf. Coat. Technol. 83 (1996) 175–182.

[14] J.W. Schultze, B. Danzfuss, O. Meyer, U. Stimmingilms, Electrochemical investigations of ion-implanted oxide films, Mater. Sci. Eng. 69 (2) (1985) 273–282.
[15] B.S. Kim, J.S. Kim, Y.M. Park, B.Y. Choi, J. Lee, Mg ion implantation on SLA-treated titanium surface and its effects on the behavior of mesenchymal stem cell, Mater. Sci. Eng. C 33 (2013) 1554–1560.
[16] J.W. Park, Y.J. Kim, J.H. Jang, H. Song, Osteoblast response to magnesium ion-incorporated nanoporous titanium oxide surfaces, Clin. Oral Implants Res. 21 (11) (2010) 1278–1287.
[17] I. Braceras, C. Vera, A.A. Izquierdo, R. Mu˜noz, J. Lorenzo, N. Alvarez, M.Á. de Maeztu, Ion implantation induced nanotopography on titanium and bone cell adhesion, Appl. Surf. Sci. 310 (2014) 24–30.
[18] E. Byon, S. Moon, S.B. Cho, C.Y. Jeong, Y. Jeong, Y.T. Sul, Electrochemical property and apatite formation of metal ion implanted titanium for medical implants, Surf. Coat. Technol. 200 (2005) 1018–1021.
[19] W.C. Clem, V.V. Konovalov, S. Chowdhury, Y.K. Vohra, S.A. Catledge, S.L. Bellis, Mesenchymal stem cell adhesion and spreading on microwave plasma–nitrided titanium alloy, J. Biomed. Mater. Res. A 76 (2) (2006) 279–287.
[20] D.M. Gordin, D. Busardo, A. Cimpean, C. Vasilescu, D. Höche, S.I. Drob, V. Mitran, M. Cornen, T. Gloriant, Design of a nitrogen-implanted titanium-based superelastic alloy with optimized properties for biomedical applications, Mater. Sci. Eng. C 33 (2013) 4173–4182.
[21] J. Park, S. Bauer, K.A. Schlegel, F.W. Neukam, K. von der Mark, P. Schmuki, TiO2 nanotube surface: 15 nm–an optimal length scale of surface topography for cell adhesion and differentiation, Small 5 (6) (2009) 666–671.
[22] K.C. Popal, L. Leoni, C.A. Grimes, T.A. Desai, The effect of TiO_2 nanotubes on endothelial function and smooth muscle proliferation, Biomaterials 30 (7) (2009) 1268–1272.
[23] A.W. Tan, B. Pingguan-Murphy, R. Ahmad, S.A. Akbar, Review of titania nanotubes: Fabrication and cellular response, Ceram. Int. 38 (2012) 4421–4435.
[24] H. Schweikl, R. Muller, C. Englert, K.A. Hiller, R. Kujat, M. Nerlich, G. Schmalz, Proliferation of osteoblasts and fibroblasts on model surfaces of varying roughness and surface chemistry, J. Mater. Sci.: Mater. Med. 18 (2007) 1895–1905.
[25] C.Y. Yang, L.Y. Huang, T.L. Shen, J.A. Yeh, Cell adhesion, morphology and biochemistry on nanotopographic oxidized silicon surfaces, Eur. Cell. Mater. 20 (2010) 415–430.
[26] E. Pecheva, L. Pramatarova, G. Altankov, Hydroxyapatite grown on a native extracellular matrix: initial interactions with human fibroblasts, Langmuir 23 (2007) 9386–9392.
[27] C.C. Chien, K.T. Liu, J.G. Duh, K.W. Chang, K.H. Chung, Effect of nitride film coatings on cell compatibility, Dental Mater. 24 (2008) 986–993.